Advances in Atmospheric Sciences
Impact Factor: 5.8
E-alert
ISSN 0256-1530
CN 11-1925/O4

Seasonal Prediction Skill and Biases in GloSea5 Relating to the East Asia Winter Monsoon

Daquan ZHANG, Lijuan CHEN, Gill M. MARTIN, Zongjian KE

Citation: Zhang, D. Q., L. J. Chen, G. M. Martin, and Z. J. Ke 2023: Seasonal Prediction Skill and Biases in GloSea5 Relating to the East Asia Winter Monsoon, *Adv. Atmos. Sci.*, 40, 2013–2028. doi: 10.1007/s00376-023-2258-8.

View online: https://doi.org/10.1007/s00376-023-2258-8

ADVANCES IN ATMOSPHERIC SCIENCES, VOL. 40, NOVEMBER 2023, 2013–2028

• **Original Paper** •

Seasonal Prediction Skill and Biases in GloSea5 Relating to the East Asia Winter Monsoon※

Daquan ZHANG[1,2], Lijuan CHEN[*1,2], Gill M. MARTIN[3], and Zongjian KE[1]

[1]*China Meteorological Administration Key Laboratory for Climate Prediction Studies*, *National Climate Centre*, *Beijing* 100081, *China*

[2]*Collaborative Innovation Center on Forecast and Evaluation of Meteorological Disasters (CIC-FEMD)*, *Nanjing University of Information Science & Technology*, *Nanjing* 210044, *China*

[3]*Met Office Hadley Centre*, *Met Office*, *Exeter EX*1 3*PB*, *UK*

(Received 13 September 2022; revised 3 January 2023; accepted 31 January 2023)

ABSTRACT

The simulation and prediction of the climatology and interannual variability of the East Asia winter monsoon (EAWM), as well as the associated atmospheric circulation, was investigated using the hindcast data from Global Seasonal Forecast System version 5 (GloSea5), with a focus on the evolution of model bias among different forecast lead times. While GloSea5 reproduces the climatological means of large-scale circulation systems related to the EAWM well, systematic biases exist, including a cold bias for most of China's mainland, especially for North and Northeast China. GloSea5 shows robust skill in predicting the EAWM intensity index two months ahead, which can be attributed to the performance in representing the leading modes of surface air temperature and associated background circulation. GloSea5 realistically reproduces the synergistic effect of El Niño–Southern Oscillation (ENSO) and the Arctic Oscillation (AO) on the EAWM, especially for the western North Pacific anticyclone (WNPAC). Compared with the North Pacific and North America, the representation of circulation anomalies over Eurasia is poor, especially for sea level pressure (SLP), which limits the prediction skill for surface air temperature over East Asia. The representation of SLP anomalies might be associated with the model performance in simulating the interaction between atmospheric circulations and underlying surface conditions.

Key words: East Asia winter monsoon (EAWM), Global Seasonal Forecast System version 5 (GloSea5), El Niño–Southern Oscillation (ENSO), prediction skill, model bias

Citation: Zhang, D. Q., L. J. Chen, G. M. Martin, and Z. J. Ke, 2023: Seasonal prediction skill and biases in GloSea5 relating to the East Asia winter monsoon. *Adv. Atmos. Sci.*, **40**(11), 2013–2028, https://doi.org/10.1007/s00376-023-2258-8.

Article Highlights:

- GloSea5 reproduces the climatology and interannual variability of EAWM index well with a two-month forecast lead time.
- Both the northern and southern modes of SAT in the EAWM region was captured well by GloSea5, despite the evolvement of systematic model bias.
- GloSea5 realistically simulates the WNPAC associated with ENSO, while the prediction skill for mid-high-latitude Eurasia is relatively low.

1. Introduction

The East Asia winter monsoon (EAWM) is one of the most active components of the global climate system during boreal winter. The EAWM exhibits strong interannual to inter-decadal variability. A strong EAWM could lead to cold extremes and snow storms in East Asia, and severe flooding in Southeast Asia, causing significant social and economic losses (Chang and Lau, 1982; Jhun and Lee, 2004; Gollan et al., 2012; Ding et al., 2014, Wang and Lu, 2017). Skillful prediction of the EAWM ahead of the upcoming season is important for the prevention and mitigation of potential losses.

The interannual variation of the EAWM is regulated by both tropical and extratropical climate factors, such as El Niño–Southern Oscillation (ENSO) (Li, 1990; Zhang et al.,

※ This paper is a contribution to the 2nd Special Issue on Climate Science for Service Partnership China.

* Corresponding author: Lijuan CHEN
Email: chenlj@cma.gov.cn

1996, 2019; Chen et al., 2000, 2019; Wang et al., 2000), the Arctic Oscillation (AO)/North Atlantic Oscillation (NAO) (Thompson and Wallace, 1998; Wu and Wang, 2002; Chen et al., 2005; He and Wang, 2013a), Arctic Sea ice (Honda et al., 2009; Wu et al., 2011; Sun et al., 2016; Fan et al., 2020), snow cover over Eurasia (Watanabe and Nitta, 1999; Wang et al., 2010), etc. The mature phase of El Niño (La Niña) events in boreal winter is usually accompanied by a weak (strong) EAWM. The anomalous low-level western North Pacific anticyclone (WNPAC) induced by ENSO plays an essential role in the relationship between ENSO and the EAWM (Wang et al., 2000; Kim et al., 2017). The southerly wind anomalies in the northwest periphery of the WNPAC tend to induce a weak EAWM. The relationship between ENSO and the EAWM also shows interdecadal variations (Zhou et al., 2007; He and Wang, 2013b), which can be attributed to the modulation effect of both the Pacific Decadal Oscillation (PDO) and Atlantic Multidecadal Oscillation (AMO) through the zonal displacement of the WNPAC (Mantua et al., 1997; Kerr, 2000; Wang et al., 2008; Kim et al., 2017). The positive phase of the AO is often related to a weak Siberian high and EAWM, which favor less intrusion by cold surges and positive surface air temperature (SAT) anomalies over East Asia, and vice versa (Gong et al., 2001; Park et al., 2011).

With the development of numerical models, the climate model has become an effective tool for understanding and projecting climate variability. Many studies have been carried out to assess the capacity of climate models in simulating and predicting the East Asian monsoon system (Sohn et al., 2011; Li and Wang, 2012; Kim et al., 2012; Jiang et al., 2013, 2020, 2022; Gong et al., 2014, 2015; Kang and Lee, 2019; Ma and Chen, 2021; Zou et al., 2022). It has been found that state-of-the-art climate models show reasonable skill in simulating the mean state of the EAWM, including the northern and southern modes of mean SAT variations over East Asia, while the performance for capturing the interannual variability is worse (Wang et al., 2010; Chen et al., 2014; Jiang et al., 2020; Li et al., 2020). Nevertheless, common deficiencies still exist, such as a systematic cold bias over East Asia (Jiang et al., 2020), weak interannual variability (Gong et al., 2014) compared with observations, an underestimated ENSO–EAWM relationship (Jiang et al., 2022), etc. The model systematic biases often develop quickly in the coupled system and have profound influences on the model capability to simulate the climate variability (Huang et al., 2007; Zhang et al., 2020a; Martin et al., 2021). The systematic drift of a model away from observations limits its prediction skill since the model drift creates a significantly different background state compared with observations and the low-frequency climate anomalies evolve based on the background state.

From these perspectives, the performance of Global Seasonal Forecast System version 5 (GloSea5) (MacLachlan et al., 2015) in simulating and predicting the EAWM and its associated large-scale circulation was examined. Previous studies have indicated that GloSea5 shows reasonable prediction skill for the EAWM on the subseasonal time scale, especially for the 1st and 2nd week (Ham and Jeong, 2021). In this study, we focus on the prediction skill for seasonal mean variability. Both the model systematic bias and the prediction skill of interannual variations of the EAWM index are investigated. The evolution of model bias with respect to the potential source of predictability (ENSO) and its impact on prediction skill is discussed. The rest of this paper is organized as follows. The data and methodology are described in section 2. Predictions of the climatology and interannual variations of both the background circulation and SAT, including the potential origin of model bias, are given in section 3. In section 4, we investigate the synergistic impact of ENSO and the AO on the EAWM in both observations and model hindcast. Conclusions and further discussions are presented in section 5.

2. Model, data, and methods

2.1. *Model description*

GloSea5 is a fully coupled climate system model that integrates atmosphere (Met Office Unified Model, MetUM; Walters et al., 2017), ocean (Nucleus for European Modeling of the Ocean, NEMO; Megann et al., 2014), sea ice (Los Alamos sea ice model, CICE; Rae et al., 2015), and land surface (Joint UK Land Environment Simulator, JULES; Best et al., 2011) components using the Ocean Atmosphere Sea Ice Soil (OASIS; Valcke, 2013) coupler. The horizontal resolution of the atmosphere and land surface components is 0.833° × 0.556°, and the ocean and sea ice models use a tripolar grid with 0.25° × 0.25° grid spacing between 20°S and 20°N and an irregular grid poleward of 20°. In this study, a 24-year research hindcast dataset of GloSea5 was investigated. The model reforecasts are initialized on 1, 9, 17, and 25 September, October, and November from 1993 to 2016. For each initial date there are seven ensemble members, each integrated for seven months, covering the EAWM active season. There are therefore a total of 28 ensemble members per year for the retrospective forecast initialized in each month. The spread of ensemble initial conditions is generated using a Stochastic Kinetic Energy Backscatter scheme (SKEB2; Bowler et al., 2009).

2.2. *Observational data*

The European Centre for Medium-Range Weather Forecasts (ECWMF) 5th-generation reanalysis product, known as ERA5 (Hersbach et al., 2020), has been used to evaluate the climatology and variability of atmospheric circulations associated with the EAWM. ERA5 replaces the ERA-interim (Dee et al., 2011) reanalysis within the Copernicus Climate Change Service (C3S). The horizontal resolution of ERA5 is 0.25° × 0.25°, with 137 vertical pressure layers extending from 1000 hPa to 0.01 hPa. The Niño-3.4 index, defined as the mean sea surface temperature anomaly in the Niño-3.4 region (Trenberth, 1997), calculated based on the

NOAA Optimum Interpolation Sea Surface Temperature version 2 (OISSTv2) dataset (Reynolds et al., 2007), and provided by Beijing Climate Center of China Meteorological Administration (BCC/CMA) (http://cmdp.ncc-cma.net/pred/cn_enso.php?product=cn_enso_nino_indices), was used to represent the variability of ENSO. The monthly mean AO index was provided by Climate Prediction Center of National Centers for Environmental Prediction (CPC/NCEP) (https://www.cpc.ncep.noaa.gov/products/precip/CWlink/daily_ao_index/ao.shtml). The AO index is constructed by projecting the 1000-mb height anomalies poleward of 20°N onto the loading pattern of the AO (Thompson and Wallace, 1998).

2.3. *Analysis methods*

Due to the complexity of the EAWM circulation system, numerous indices have been proposed to measure its intensity (Wang and Chen, 2010, 2014), with focus on the lower (surface), middle, and upper tropospheric circulation associated with the EAWM, respectively. Considering both model performance and the relationship between EAWM and surface temperature, the EAWM index developed by Zhu (2008) was selected for this study; hereafter, EAWM index refers to the EAWM index developed by Zhu (2008). The EAWM index is defined as the standardized mean horizontal shear of the 500-hPa zonal winds, and it reflects the integrated influence of the atmospheric circulation over low and high latitudes and the thermal difference between the ocean and continent. The EAWM index shows significant correlations with winter mean temperature over China, as compared with the index proposed by Li and Yang (2010), which is defined by the mean wind shear of the upper-tropospheric zonal wind.

$$I_{\mathrm{EAWM}} = \bar{U}_{500}(25°-35°\mathrm{N}, 80°-120°\mathrm{E}) - \bar{U}_{500}(50°-60°\mathrm{N}, 80°-120°\mathrm{E}) .$$

The EAWM index used in this study was calculated based on the seasonal mean zonal wind at 500 hPa during boreal winter (December to February). Empirical orthogonal function (EOF) analysis was performed to obtain the leading modes of spatialtemporal variations of SAT over East Asia and sea level pressure (SLP) over the Northern Hemisphere poleward of 20°N. Correlation and regression analysis were utilized and a two-tailed Student's *t*-test was performed to test the statistical significance. Additionally, composite analysis was performed on both observational and model hindcast results with respect to different combinations of ENSO and AO phases in boreal winter. The model bias refers to GloSea5 minus ERA5 hereafter.

3. Simulation and prediction of the EAWM

3.1. *Climatology*

The EAWM is characterized by a continental-scale high pressure system centered in Siberia (SH) and strong surface northerlies due to the strong west–east pressure gradient between the SH and the Aleutian low (Fig. 1a). The EAWM is also related to the East Asian trough (EAT) in the mid troposphere and the East Asian jet stream (EAJS) in the upper troposphere (Fig. 1d). The performance of GloSea5 in representing these circulation systems was evaluated. The wintertime mean circulations over East Asia from the GloSea5 ensemble mean reforecast with all initial dates between September and November and their deviations from observations are given. The GloSea5 hindcast represents the climato-

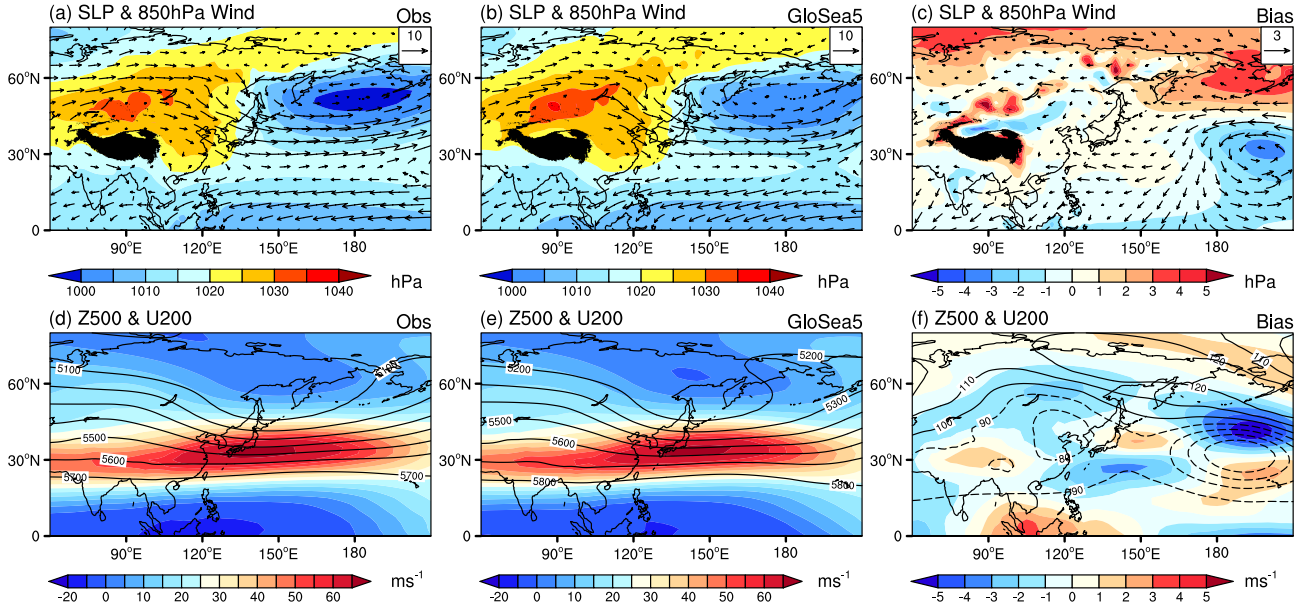

Fig. 1. Climatology of winter mean (a) SLP (shading, hPa) and 850-hPa horizontal winds (vectors, m s^{-1}), (d) The 500-hPa geopotential height (Z500, contours, contour interval = 100 gpm), and 200-hPa zonal wind (U200, shading, m s^{-1}) in ERA5. (b), (e) as in (a), (d), but for GloSea5 hindcasts initiated in November. (c) The model bias for SLP and 850-hPa wind. (f) The mode bias for Z500 and zonal wind at 200 hPa (contour interval = 10 gpm).

logical characteristics of the circulations associated with the EAWM well. Nevertheless, GloSea5 shows systematic biases, such as higher SLP to the west of Lake Baikal and around the Aleutian Islands (Fig. 1c), indicating a stronger SH and weaker Aleutian low compared with observations. GloSea5 also shows a salient positive bias for 500-hPa geopotential height fields (hereafter referred to as Z500) in high latitudes and over the Ural Mountains, corresponding to a weaker AO and stronger Ural blocking high. The EAT in GloSea5 is weaker than that seen in observations, which is associated with the reduced gradient between the mid and high latitudes. Moreover, the predicted zonal wind along the westerly jet stream is weaker than observations and shifted southward near Japan, except for the part over the eastern North Pacific and Tibetan Plateau (Fig. 1f).

The wintertime 2-m air temperature (T2m) over China in GloSea5 shows a cold bias for most of East China, with the maximum bias over Northeast and North China (Fig. 2). Positive biases are found over the southeastern Tibetan Plateau and southern Xinjiang. The systematic cold bias over East China is a common deficiency for most CMIP5 models, although there is some improvement in CMIP6 (Gong et al., 2014; Wei et al., 2014; Jiang et al., 2020). The cold bias is closely related to the model errors in the large-scale atmospheric circulation. Previous studies (Wu and Wang, 2002) have revealed that both a weak AO and a strong SH favor a strong EAWM and frequent cold surge intrusions into East Asia. The wintertime blocking near the Ural Mountains also reinforces the SH and enhances southward cold advection, contributing to the cold bias in China, which might be associated with a stronger Atlantic jet stream (Cheung and Zhou, 2015). On the other hand, the cold bias is most significant in hindcasts initialized in November, and the associated circulations and possible explanations will be discussed in the following section.

3.2. *Interannual variability*

The above analysis indicates that the main climatological features of atmospheric circulation systems associated with the EAWM can be simulated well by GloSea5, despite significant systematic model biases. The prediction skill for the interannual variation of the EAWM index by GloSea5 with different lead times was evaluated. Both the observed and GloSea5-predicted EAWM intensity index exhibit strong interannual variability (Fig. 3). Despite the relatively big ensemble spread, the ensemble mean forecasts of EAWM intensity are in good accordance with observed values in most years. The temporal correlation coefficient (TCC) reaches 0.56 for forecasts initiated in October, exceeding the 99% confidence level based on the Student *t*-test. Note that with the shortest lead time, the correlation coefficient of forecasts initiated in November is 0.14, smaller than that initiated in October.

The spatial distribution of TCCs between GloSea5-predicted T2m with different lead times and observations is shown in Fig. 4. Similar to the EAWM index, the forecasts initiated in October show the highest prediction skill, with the TCCs in most regions of East China, except Northeast China, exceeding the 90% confidence level. The prediction skill of hindcasts initiated in November is the poorest among all three months, with the smallest area of TCCs passing the significance test. The distributions of TCCs of forecasts initiated in September and October show similar spatial patterns, with better performance in the Yangtze River valley and relatively low prediction skill in Northeast and Southwest China. However, the distribution of TCCs of forecasts initiated in November is quite different; only parts of North China and Southwest China pass the significance test.

3.3. *Prediction of leading temperature modes and associated circulations*

Previous studies have indicated that two distinct modes, i.e., the northern and southern modes, dominate the interannual variation of SAT in the EAWM region (0°–60°N, 100°–140°N) (Kang et al., 2006, 2009; Wang et al., 2010; Sohn et al., 2011; Gong et al., 2018; Zou et al., 2022). The associated atmospheric circulation and climate factors of each mode are different, with the southern mode being more related to tropical factors such as ENSO, and the northern mode being primarily associated with mid-high-latitude circulation and underlying surface factors, such as Eurasian snow cover (Wang et al., 2010) and Arctic sea ice (Zhang et al., 2020b).

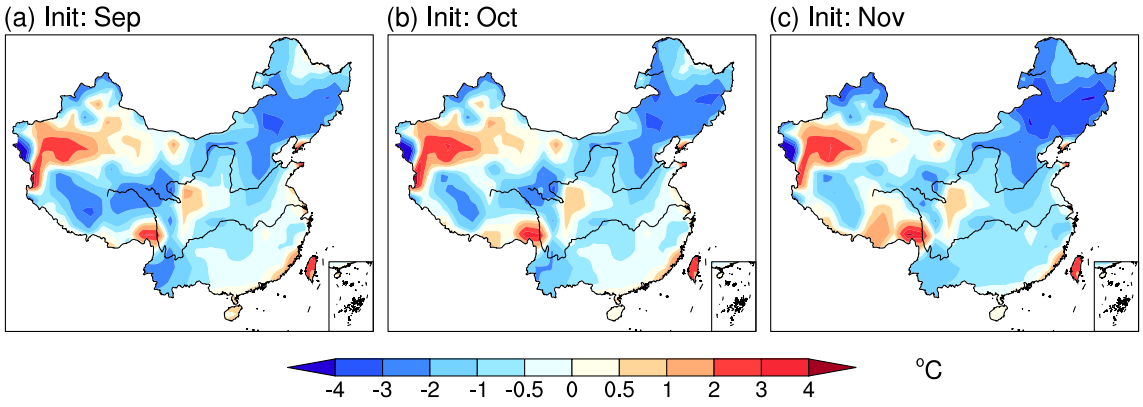

Fig. 2. Differences between climatological (1993–2016) wintertime mean T2m (°C) in GloSea5 initiated in September (a), October (b), and November (c) and ERA5.

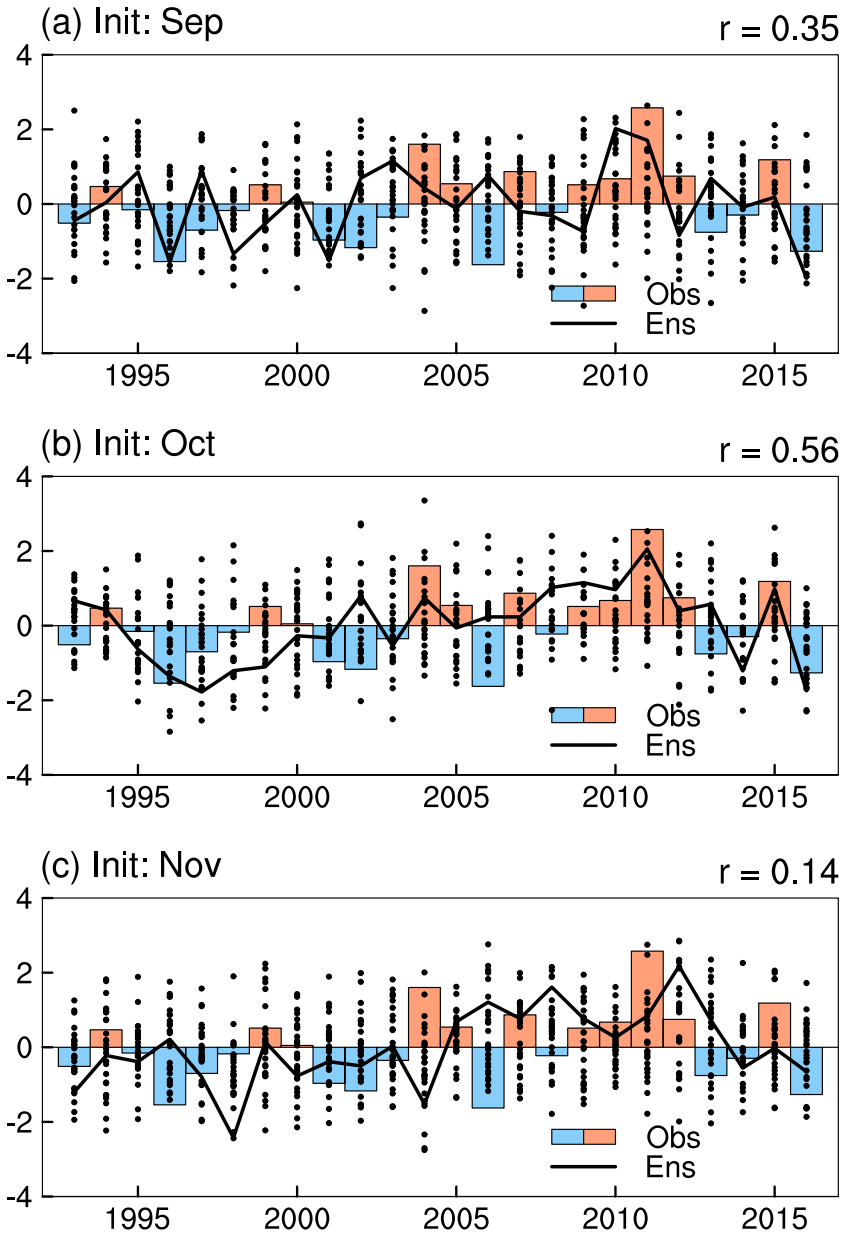

Fig. 3. Interannual variation of the EAWM intensity index predicted by GloSea5 forecasts initiated in September (a), October (b), and November (c). The interannual variation from observations is shown by the bars. Black lines denote the model ensemble mean, while black dots denote individual ensemble members. *r* indicates the TCC between observations and ensemble mean predictions. The years marked on the horizontal axis correspond to the start month of each winter (DJF), i.e., 1993–2016 corresponds to 1993/94–2016/17.

The performance of GloSea5 in representing the dominant modes of temperature in the EAWM region and associated large-scale background circulation was examined. EOF analysis was performed on the winter mean T2m anomalies in the EAWM region for both observations and GloSea5 hindcasts. The two leading modes (EOF1, EOF2) of observed T2m explain 74.1% of the total variance, which is similar to the results of previous studies (73.7%, Wang et al., 2010). The northern mode (EOF1) features a cold winter in northeast Asia (Fig. 5a), and the southern mode (EOF2) displays a cooling center in southern Mongolia while the negative anomalies extend from northwest Mongolia to the South China Sea (SCS) (Fig. 5e). The spatial pattern of the northern mode is simulated well by GloSea5, despite its deviation in intensity between different forecast lead times. It should be noted that a significant cold bias center in Mongolia can be found in hindcasts initiated in November (Fig. 5d), which might be associated with the poor prediction skill illustrated in Fig. 2c. Meanwhile, the explained variance of the northern mode is lower compared with observations (Figs. 5b, c, and

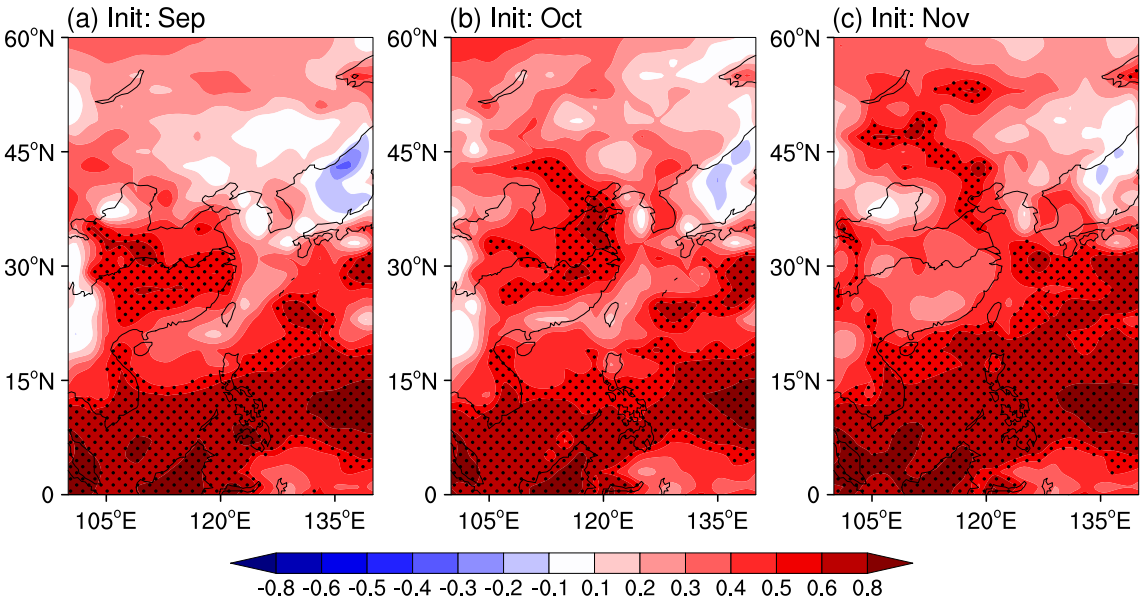

Fig. 4. TCCs between the observations and GloSea5-predicted interannual variation of winter mean T2m (°C) for forecasts initiated in September (a), October (b), and November (c). The dotted area is significant at the 90% confidence level.

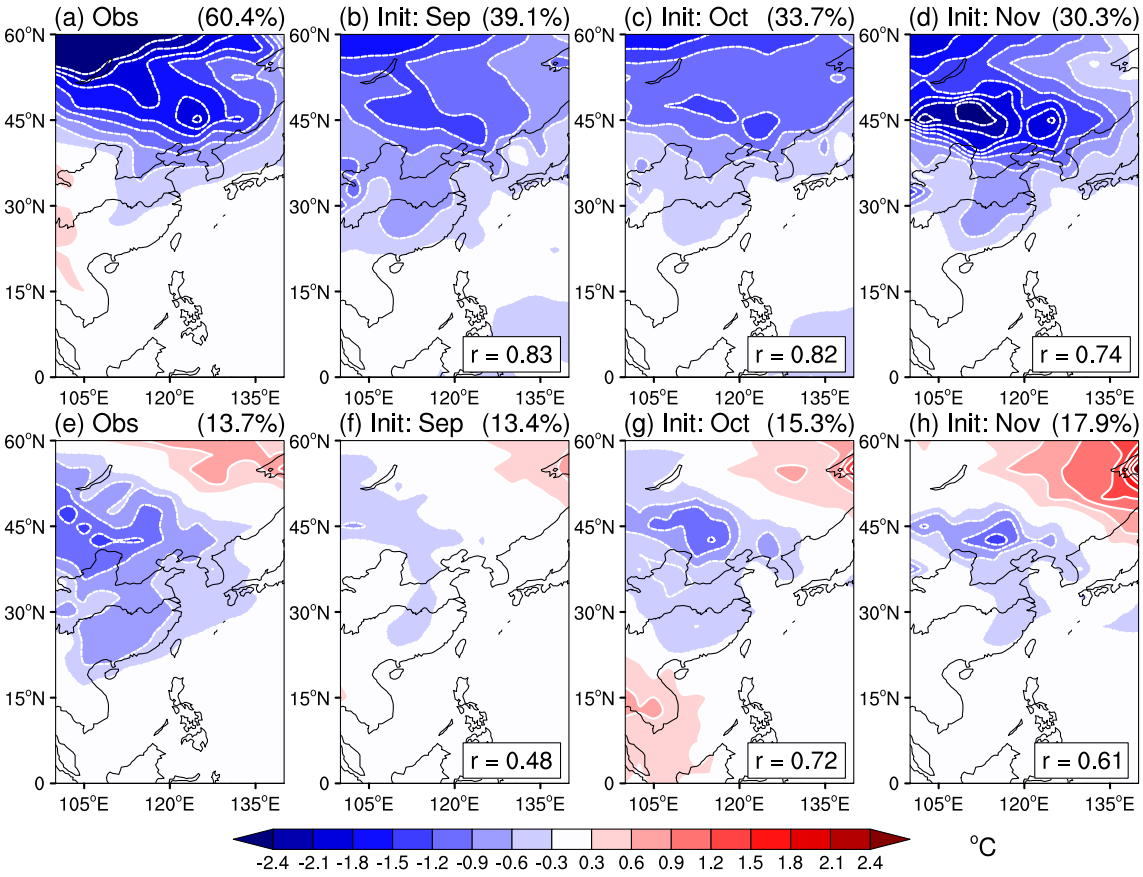

Fig. 5. (a), (e) Spatial patterns of the first and second EOF mode of winter mean T2m (shading, °C) over East Asia (0°–60°N, 100°–140°E) in ERA5. (b), (f) as in (a), (e) but for GloSea5 predictions initiated in September. (c), (g) and (d), (f) as in (b), (f) but for October and November. Values in parentheses denote percentages of explained variances in ERA5 and GloSea5 hindcasts. *r* in the lower right corner of each graph indicates the pattern correlation coefficients between observed and predicted modes.

d). On the other hand, GloSea5 captures the spatial patterns of the southern mode for hindcasts initiated in October and November, but it shows poor representation in September (Figs. 5f, g, and h). On the whole, hindcasts initiated in October show the highest forecasting skill in representing both the northern and southern mode, which is consistent with the EAWM index (Fig. 3).

The prediction skill of GloSea5 for the interannual variations of two temperature modes was investigated (Fig. 6). As introduced in section 2.1, there are four initialization dates in each month and seven ensemble members for each forecast. Although GloSea5 can reproduce the spatial patterns of the northern and southern modes well, the prediction skill for its interannual variations is moderate. The correlation coefficient between observations and GloSea5 hindcasts for the northern mode is higher than for the southern mode, in general. The prediction skill of both the northern and southern mode from GloSea5 shows an overall increasing trend with decreased forecast lead time.

As revealed in previous studies, the positive phase of the northern mode is related to a westward displacement of the EAT and an enhanced SH (Wang et al., 2010; Cheung et al., 2012). Regression analysis shows that the northern mode is also characterized by a positive center of SLP anomalies over the Ural Mountains, accompanied by a "warm Arctic –cold Eurasia" (Mori et al., 2014) like spatial pattern of T2m (Fig. 7a). In the mid-troposphere, a major ridge can be found near the Ural Mountains, with a strong lower pressure anomaly centered near Lake Baikal (Fig. 7b), which favors a cold air outbreak toward northeast Asia. Positive anomalies of zonal wind at 200 hPa can be found in midlatitude East Asia, indicating a strong EAJS (Ham and Jeong, 2021).

GloSea5 successfully captures the high pressure center over the Ural Mountains, but fails to reproduce the "warm Arctic–cold Eurasia" pattern of T2m seen in observations, with an overall negative anomaly for both the mid and high latitudes (Fig. 7c, e, and g). GloSea5 also realistically reproduces the location of the major trough and ridge over Eurasia, with increasing amplitude for shortened forecast lead time (Fig. 7d, f, and h). The enhanced ridge along the Ural Mountains and the trough over Lake Baikal and Northeast Asia favor cold air outbreaks, contributing to the increased cold bias for shorter forecast lead time, especially in North and Northeast China. There are negative anomalies north of 30°N and positive anomalies south of 30°N for GloSea5-predicted zonal wind at 200 hPa, indicating a systematic southward shift of the EAJS compared with observations. Moreover, a significant negative model bias can be found in both SLP and Z500 over the eastern North Pacific.

For the southern mode, cold air occupies Eurasia south of 50°N, especially in East Asia (Fig. 8a). In observations, a salient SLP ridge extends from Mongolia along the eastern flank of the Tibetan Plateau to the SCS. The spatial distribution of Z500 anomalies over Eurasia shows a meridional dipole mode between middle and high latitudes (Fig. 8b). The negative Z500 anomalies near Japan correspond to a deepened East Asian trough. In the upper troposphere, the EAJS is intensified with positive zonal wind anomalies extending from the Arabian Peninsula to Japan along 30°N. The performance of GloSea5 in simulating the circulation structures associated with southern mode is relatively poor compared with the northern mode. Only hindcasts initiated in October capture the spatial distribution of SLP anomalies, deepening of the EAT, and intensified EAJS, consistent with the well-simulated southern mode (Fig. 5g), which explains the higher prediction skill for both the EAWM index and T2m anomalies. The meridional dipole mode of Z500 anomalies over Eurasia and spatial pattern of anomalous zonal wind at 200 hPa were reproduced well in hindcasts initiated in October, consistent with the relatively higher prediction skill for the EAWM index (Zhu, 2008). The prediction skill for the EAWM index (Li and Yang, 2010) shown by GloSea5 initiated in October is also the highest compared to forecast initiated in September or November (figure not shown); recall that the EAWM index is defined by the shear of the zonal wind 200 hPa.

In addition, significant systematic biases can be found over Eurasia North Pacific for Z500. In hindcasts initiated in September, GloSea5 fails to represent the meridional dipole structure over Eurasia and exhibits significant negative bias over the eastern North Pacific (Fig. 8d). For November, the positive center in northern Eurasia disappears, while a pos-

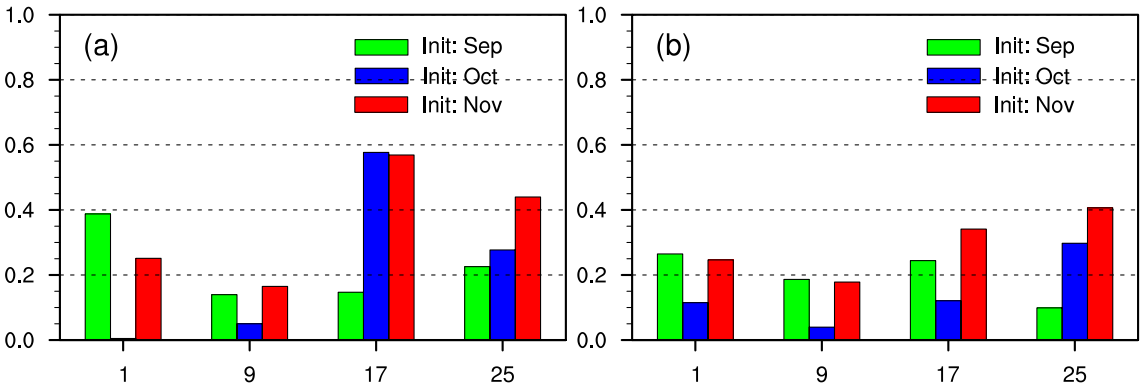

Fig. 6. The TCCs between time series associated with EOF1 (a), EOF2 (b) in ERA5 and GloSea5 hindcasts initiated on 1, 9, 17, and 25 September (green), October (blue), and November (red), respectively.

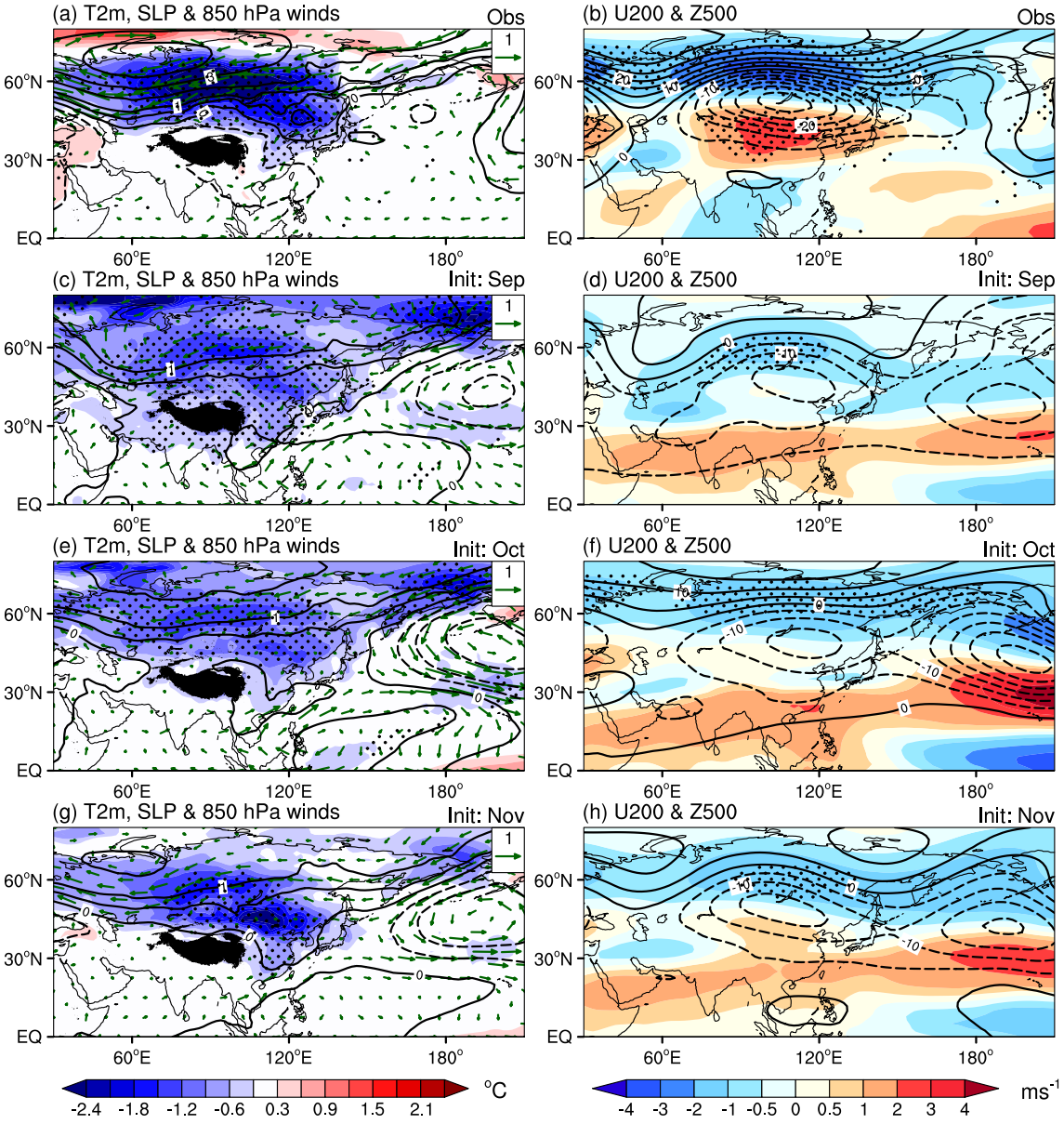

Fig. 7. Regressed winter mean (left) T2m (shading, °C), SLP (contours, hPa), horizontal winds at 850 hPa (vector, m s^{-1}) and (right) zonal wind at 200 hPa (U200, shading, m s^{-1}), 500-hPa geopotential height (Z500, contours, gpm) anomalies with respect to PC1 from observations (a, b) and GloSea5 hindcasts initiated in September (c, d), October (e, f), November (g, h), respectively. Dotted areas in the left (right) column denote regressed T2m (U200) being significant at the 95% confidence level.

itive center of Z500 (Fig. 8h) and anticyclonic circulation anomalies in the lower troposphere can be found over the North Pacific, contributing to the warm bias of Northeast Asia and the Sea of Okhotsk (Fig. 8g).

4. Combined effects of ENSO and the AO on the EAWM

As the strongest mode of the tropical Pacific air–sea coupled system on the seasonal and interannual time scales, the relationship between the EAWM and ENSO has been extensively discussed in previous studies (He and Wang, 2013b; Gong et al., 2018, Ham and Jeong, 2021). The anomalous low-level anticyclone in the western North Pacific associated with El Niño plays an important role since the southerlies on its western flank lead to warm advection to East Asia and attenuate the EAWM (Kang and Lee, 2019). GloSea5 shows robust prediction skill for ENSO variability, and the anomaly correlation coefficient is over 0.8 for a five-month lead time (MacLachlan et al., 2015). In order to evaluate the model performance in simulating the relationship between ENSO and the EAWM, composite analyses were performed on both observations and GloSea5 seasonal hindcasts of DJF for El Niño and La Niña years from 1993 to 2016, respectively (Fig. 9). The ENSO-related years are selected based on the mean Niño-3.4 index in boreal winter and classified

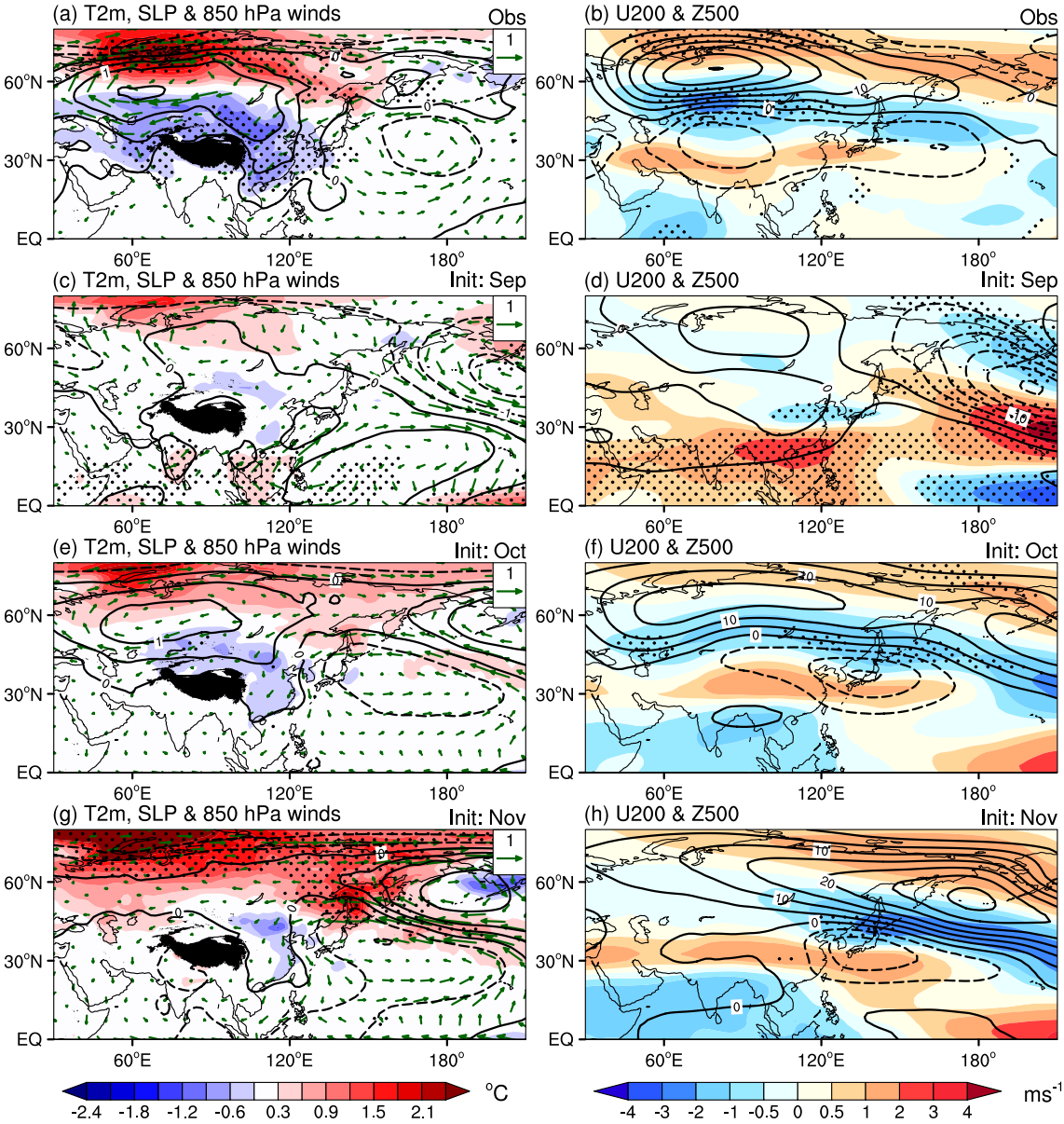

Fig. 8. The same as Fig. 7 but for PC2.

into El Niño (≥0.5°C) and La Niña years (≤−0.5°C), respectively. The El Niño years are 1994, 1997, 2002, 2006, 2009, 2014, and 2015; La Niña years are 1995, 1996, 1998, 1999, 2000, 2005, 2007, 2008, 2010, and 2011. The selected years correspond to the start month of each winter (December–February), i.e., 1994 correspond to the 1994/95 winter.

In El Niño years, a significant anomalous cyclone and negative anomalies in Z500 can be found over the North Pacific, both associated with the positive phase of the Pacific–North American (PNA) pattern (Wallace and Gutzler, 1981). There exist a trough along the Ural Mountains and a ridge extending from Lake Baikal to Lake Balkhash, resulting in above normal T2m over north and East Asia (Fig. 9a). The distribution of anomalous circulation is roughly the opposite during La Niña years (Fig. 9b), despite the relatively weaker anomalous cyclone over the western North Pacific compared to its counterpart in El Niño years. Note that compared with the Pacific and North American sections, the composite result of T2m anomalies over East Asia shows no statistical significance for both El Niño and La Niña years.

GloSea5 captures the spatial distributions of both T2m and circulation anomalies over the Pacific and North America well, with a positive bias in T2m over the central and eastern Pacific for El Niño years (Figs. 9c, e, and g) and a negative bias in La Niña years (Figs. 9d, f, and h). The WNPAC associated with ENSO is simulated well by GloSea5 for different forecast lead times. However, the simulation of atmospheric response to ENSO is poor in the mid-high latitudes of Eurasia. A negative center of Z500 can be found over North Europe and positive T2m anomalies are located over Eastern

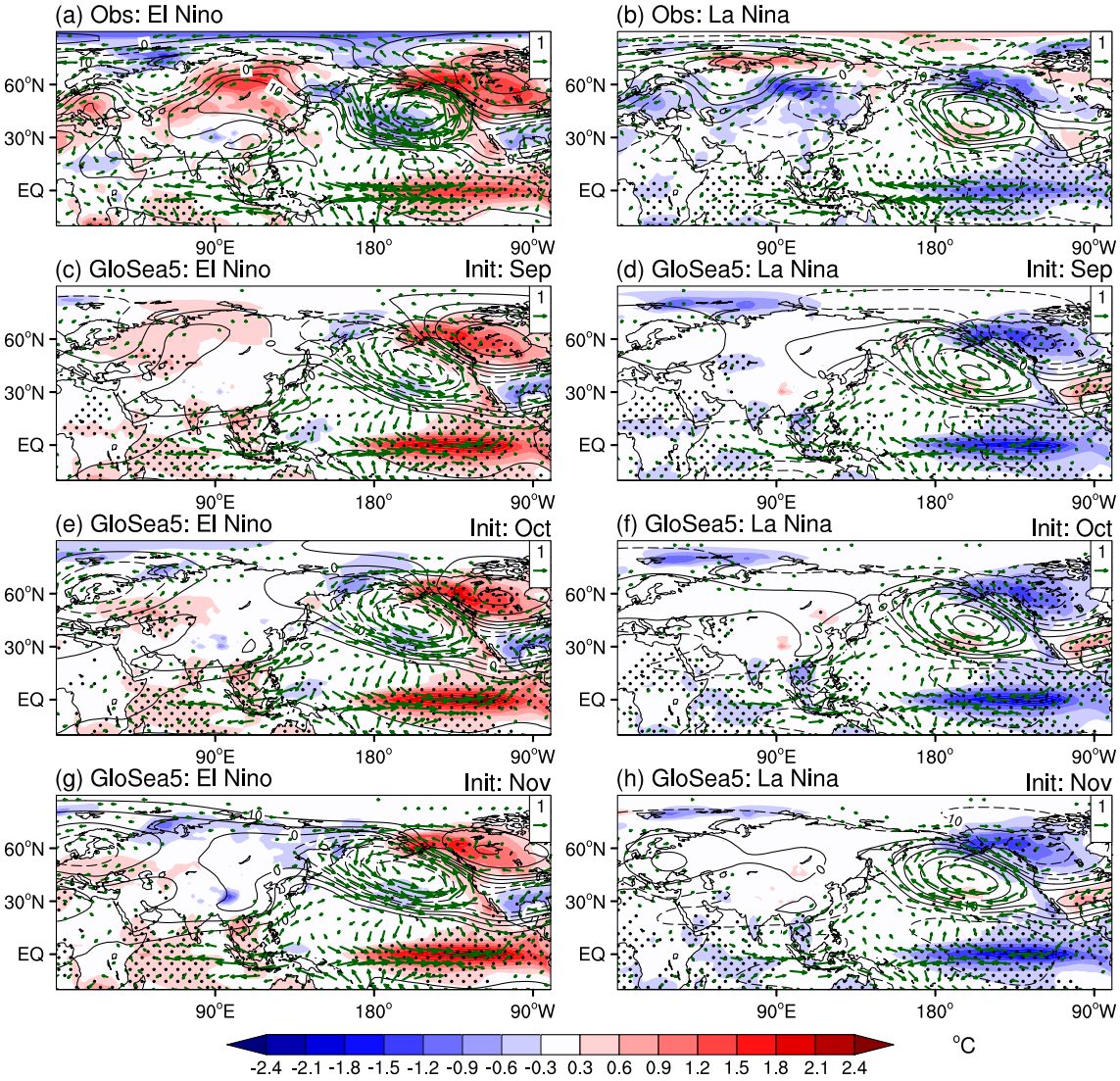

Fig. 9. Composite of winter mean T2m (shading, °C), horizontal winds at 850 hPa (green vector, m s^{-1}), and 500-hPa geopotential height (contours, gpm) anomalies with respect to El Niño (left) and La Niña (right) years from 1993 to 2016 for observations (a, b) and GloSea5 hindcasts initiated in September (c, d), October (e, f), and November (g, h), respectively. Dotted areas denote the composite of T2m anomalies is significant at the 95% confidence level.

Europe and western Asia for El Niño years. GloSea5 fails to reproduce the spatial distributions of T2m and circulations anomalies associated with La Niña events.

Outside the tropics, the AO is key to explaining the interannual variations of the EAWM and surface temperature over Eurasia (Gong et al., 2001). Previous studies have shown a highly significant level of prediction skill for the interannual variability of the AO with a one-month forecast lead time (Scaife et al., 2014; MacLachlan et al., 2015). Nevertheless, GloSea5 shows a systematic bias in the spatial patterns of SLP associated with the AO (Fig. 10). The explained variance of the leading mode is higher than the observational result. The positive SLP anomaly center in the North Atlantic is weaker and shows a westward displacement compared to observations, while the positive center in North Pacific is stronger than observations. The overestimated magnitude of the Pacific center in the wintertime AO pattern is a common bias in CMIP5 models, which might be associated with the model errors in ENSO-related teleconnections and sea ice (Cattiaux and Cassou, 2013; Gong et al., 2017).

Finally, the combined effects of ENSO and the AO on the winter atmospheric circulation of the Northern Hemisphere in both observation and GloSea5 hindcasts were investigated. Compared with ENSO, the AO exhibits higher frequency variability and could change significantly during one winter. Following Chen et al. (2013), the monthly anomalies of the AO are taken into consideration for all El Niño and La Niña winters. When an El Niño event couples with positive AO phases, a negative SLP anomaly occupies the polar region and northwest Asia, denoting a weak SH. A trough is seen over the Ural Mountains and a significant positive center exists over Northeast Asia, favoring a weak EAWM and warm anomalies in northern China (Fig. 11a). When a La Niña event couples with negative AO phases, a

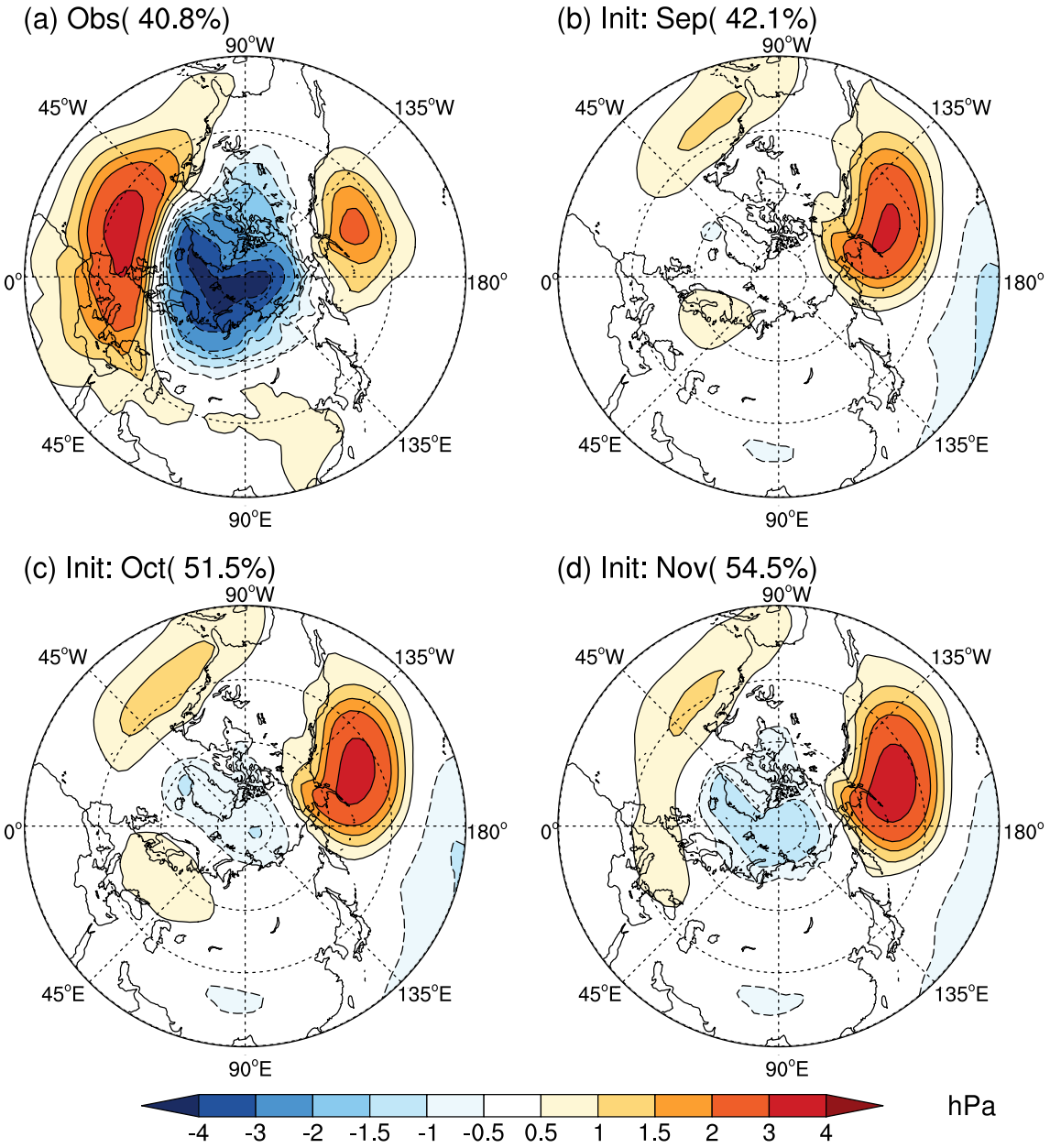

Fig. 10. Leading EOF mode of winter mean SLP (shading, hPa) anomalies poleward of 20°N for observations (a) and GloSea5 hindcasts initiated in September (b), October (c), and November (d), respectively.

stronger SH and more Ural blocking favor frequent outbreaks of cold air toward East Asia, resulting in cold anomalies over northern China (Fig. 11g) (Cheung et al., 2012; Qiao et al., 2020). However, when an El Niño event couples with negative AO phases, or a La Niña event couples with positive AO phases, the centers of atmospheric response in the mid-high latitudes are mainly located in the Western Hemisphere (Figs. 11c and e). The nonlinear characteristics of the combined impact of ENSO and the AO on the winter climate of East Asia can be attributed to the interaction between the troposphere and stratosphere, and the middle-low-latitude interaction (Chen et al., 2013; Qiao et al., 2021).

GloSea5 reproduces the spatial distributions of atmospheric response for different combinations of ENSO and the AO well, but with a generally underestimated intensity. The results of the composite analysis based on GloSea5 hindcasts initiated in November are given in Fig. 11, and similar spatial patterns are seen for September and October (figures not shown). The prediction skill for SLP is relatively lower than that for Z500, especially in the mid-high latitudes. GloSea5 fails to reproduce the SLP anomalies over Eurasia associated with ENSO and the AO. The most significant model deviation from observation is the positive bias in the Arctic region for El Niño and a positive AO (Fig. 11b), which is consistent with the systematic bias in SLP with respect to the AO (Figs. 10b, c, and d). In the midlatitudes, GloSea5 overestimates the positive pressure center near the Aleutian Peninsula and shows a reverse dipole structure in

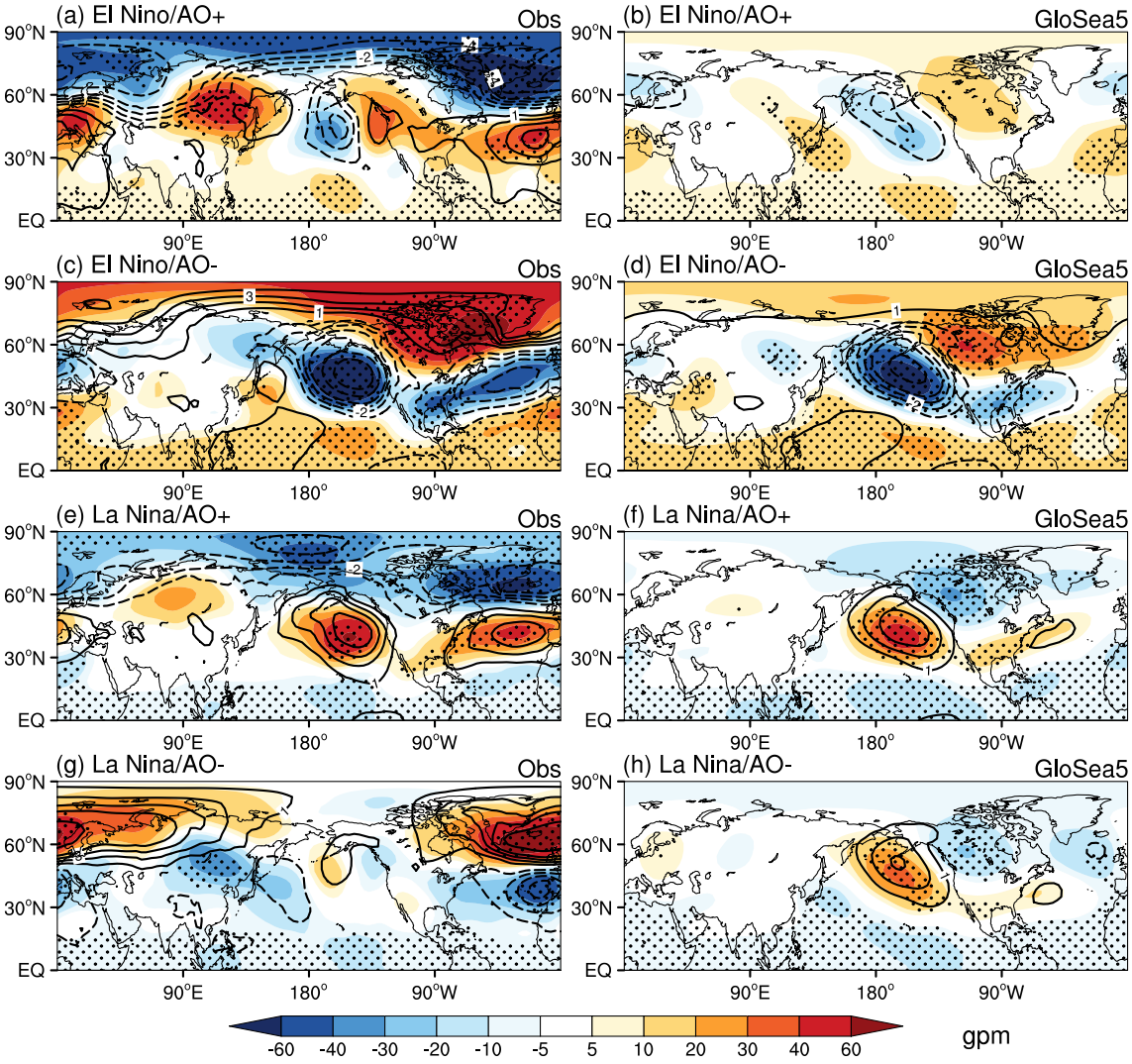

Fig. 11. Composite of Z500 (shading, gpm) and SLP (contours, hPa) anomalies in the Northern Hemisphere for (a) months with a positive AO during El Niño winter, (c) months with a negative AO during El Niño winter, (e) months with a positive AO during La Niña winter, and (g) months with a negative AO during La Niña winter from observations. (b), (d), (f), (h) as in (a), (c), (e), (f) but for GloSea5 hindcasts initiated in November. Dotted areas denote composite of Z500 anomalies is significant at the 95% confidence level.

the North Atlantic for La Niña events coupled with negative AO phases.

5. Summary and discussion

In this study, the simulation and prediction of EAWM intensity and the associated atmospheric circulations were investigated, including the climatology, interannual variability, dominant modes, and relationship with tropical and extratropical climate factors, using hindcast data from GloSea5 for winters during the period 1993–2016, with focus on the evolution of systematic model bias. The large-scale background circulations associated with the EAWM are simulated well, despite significant model errors. The cold bias over most of China's mainland is closely linked to the weak polar vortex, enhanced SH, and increased Ural blocking in GloSea5 compared with observations, which is a common deficiency in most CMIP5 and CMIP6 models. GloSea5 also simulated the northern and southern modes of surface temperature in the EAWM region well, including its associated atmospheric circulations.

In addition, the performance of GloSea5 in predicting the interannual variation of the DJF mean EAWM index and T2m in China was evaluated with respect to different forecast lead times. GloSea5 shows significant prediction skill for the EAWM intensity index two months ahead, and the TCC between the ensemble mean EAWM index and observation is 0.56, which is significant at 99% confidence level. This highly significant level of prediction skill can be attributed to the model capability in simulating the spatial patterns of surface temperature and circulations of both the northern and southern mode. Nonetheless, the prediction skill decreased for hindcasts initialized in November, which might be related to the poor representation of atmospheric cir-

culation associated with the southern mode.

Furthermore, comparative analysis was performed to evaluate the prediction skill for the EAWM under different backgrounds of ENSO and the AO, including its synergistic effects. The ENSO-related teleconnections are simulated well, including the WNPAC, which serves as a key system in bridging ENSO and East Asia climate. However, the prediction skill for circulation anomalies over the mid-high latitudes of Eurasia is poor, especially for La Niña winters. Although GloSea5 captures the spatial pattern of circulation over North America and the Atlantic sector, significant model bias exists, especially for the SLP in the Arctic region in El Niño winters coupled with a positive AO, and La Niña winters coupled with a negative AO. Previous studies have revealed the important role of Arctic sea ice (Wu et al., 2011; Zhang et al., 2020b) and Eurasian snow (Wang et al., 2010) in regulating the EAWM and surface temperature of Eurasia. The simulation of interactions between sea ice, snow cover, and the atmosphere needs to be taken into consideration in the model assessment. Additionally, the ENSO–EAWM relationship is not stationary and shows significant interdecadal variations (Zhou et al., 2007; Wang et al., 2008; Ham and Jeong, 2021), which are beyond the scope of this study and need further investigation

Acknowledgements. This research was jointly supported by the State Key Program of the National Natural Science of China (Grant No. 41730964), the National Key Research and Development Program on Monitoring, Early Warning and Prevention of Major Natural Disaster (2018YFC1506000), the National Natural Science Foundation of China (Grant Nos. 41975091 and 42175047), National Basic Research Program of China (2015CB453203), and UK-China Research & Innovation Partnership Fund through the Met Office Climate Science for Service Partnership (CSSP) China as part of the Newton Fund.

Data availability. The GloSea5 data used in this study are archived at the Met Office and are available to research collaborators upon request. The ERA5 reanalysis data are available at https://cds.climate.copernicus.eu. The monthly Niño-3.4 index can be downloaded from the official website of BCC/CMA at http://cmdp.ncc-cma.net/pred/cn_enso.php?product=cn_enso_nino_indices. The monthly AO index, which extends from 1950 to 2022, is available at https://www.cpc.ncep.noaa.gov/products/precip/CWlink/daily_ao_index.

REFERENCES

Best, M. J., and Coauthors, 2011: The Joint UK Land Environment Simulator (JULES), model description-Part 1: Energy and water fluxes. *Geoscientific Model Development*, **4**(3), 677–699, https://doi.org/10.5194/gmd-4-677-2011.

Bowler, N. E., A. Arribas, S. E. Beare, K. R. Mylne, and G. J. Shutts, 2009: The local ETKF and SKEB: Upgrades to the MOGREPS short-range ensemble prediction system. *Quart. J. Roy. Meteor. Soc.*, **135**(640), 767–776, https://doi.org/10.1002/qj.394.

Cattiaux, J., and C. Cassou, 2013: Opposite CMIP3/CMIP5 trends in the wintertime Northern Annular mode explained by combined local sea ice and remote tropical influences. *Geophys. Res. Lett.*, **40**(14), 3682–3687, https://doi.org/10.1002/grl.50643.

Chang, C. P., and K. M. Lau, 1982: Short-term planetary-scale interactions over the tropics and midlatitudes during northern winter. Part I: Contrasts between active and inactive periods. *Mon. Wea. Rev.*, **110**(8), 933–946, https://doi.org/10.1175/1520-0493(1982)110<0933:STPSIO>2.0.CO;2.

Chen, W., H. F. Graf, and R. H. Huang, 2000: The interannual variability of East Asian winter monsoon and its relation to the summer monsoon. *Adv. Atmos. Sci.*, **17**(1), 48–60, https://doi.org/10.1007/s00376-000-0042-5.

Chen, W., S. Yang, and R.-H. Huang, 2005: Relationship between stationary planetary wave activity and the East Asian winter monsoon. *J. Geophys. Res.: Atmos.*, **110**(D14), D14110, https://doi.org/10.1029/2004JD005669.

Chen, W., X. Q. Lan, L. Wang, and Y. Ma, 2013: The combined effects of the ENSO and the Arctic Oscillation on the winter climate anomalies in East Asia. *Chinese Science Bulletin*, **58**(12), 1355–1362, https://doi.org/10.1007/s11434-012-5654-5.

Chen, W., L. Wang, J. Feng, Z. P. Wen, T. J. Ma, X. Q. Yang, and C. H. Wang, 2019: Recent progress in studies of the variabilities and mechanisms of the East Asian monsoon in a changing climate. *Adv. Atmos. Sci.*, **36**(9), 887–901, https://doi.org/10.1007/s00376-019-8230-y.

Chen, Z., R. G. Wu, and W. Chen, 2014: Distinguishing interannual variations of the northern and southern modes of the East Asian winter monsoon. *J. Climate*, **27**(2), 835–851, https://doi.org/10.1175/JCLI-D-13-00314.1.

Cheung, H. H. N., and W. Zhou, 2015: Implication of Ural blocking for East Asian winter climate in CMIP5 GCMs. Part I: Biases in the historical scenario. *J. Climate*, **28**(6), 2203–2216, https://doi.org/10.1175/JCLI-D-14-00308.1.

Cheung, H. N., W. Zhou, H. Y. Mok, and M. C. Wu, 2012: Relationship between Ural-Siberian blocking and the East Asian winter monsoon in relation to the Arctic Oscillation and the El Niño-Southern Oscillation. *J. Climate*, **25**(12), 4242–4257, https://doi.org/10.1175/JCLI-D-11-00225.1.

Dee, D. P., and Coauthors, 2011: The ERA-Interim reanalysis: Configuration and performance of the data assimilation system. *Quart. J. Roy. Meteor. Soc.*, **137**(656), 553–597, https://doi.org/10.1002/qj.828.

Ding, Y. H., and Coauthors, 2014: Interdecadal variability of the East Asian winter monsoon and its possible links to global climate change. *J. Meteor. Res.*, **28**(5), 693–713, https://doi.org/10.1007/s13351-014-4046-y.

Fan, H. D., L. Wang, Y. Zhang, Y. M. Tang, W. S. Duan, and L. Wang, 2020: Predictable patterns of wintertime surface air temperature in Northern Hemisphere and their predictability sources in the SEAS5. *J. Climate*, **33**(24), 10 743–10 754, https://doi.org/10.1175/JCLI-D-20-0542.1.

Gollan, G., R. J. Greatbatch, and T. Jung, 2012: Tropical impact on the East Asian winter monsoon. *Geophy. Res. Lett.*, **39**(17), L17801, https://doi.org/10.1029/2012GL052978.

Gong, D.-Y., S.-W. Wang, and J.-H. Zhu, 2001: East Asian winter monsoon and Arctic Oscillation. *Geophys. Res. Lett.*, **28**(10), 2073–2076, https://doi.org/10.1029/2000GL012311.

Gong, H. N., L. Wang, W. Chen, X. L. Chen, and D. Nath, 2017: Biases of the wintertime Arctic Oscillation in CMIP5 models. *Environmental Research Letters*, **12**(1), 014001, https://

doi.org/10.1088/1748-9326/12/1/014001.

Gong, H. N., L. Wang, W. Chen, R. G. Wu, K. Wei, and X. F. Cui, 2014: The climatology and interannual variability of the East Asian winter monsoon in CMIP5 models. *J. Climate*, **27**(4), 1659–1678, https://doi.org/10.1175/JCLI-D-13-00039.1.

Gong, H. N., L. Wang, W. Chen, D. Nath, G. Huang, and W. C. Tao, 2015: Diverse influences of ENSO on the East Asian-Western Pacific winter climate tied to different ENSO properties in CMIP5 models. *J. Climate*, **28**(6), 2187–2202, https://doi.org/10.1175/JCLI-D-14-00405.1.

Gong, H. N., L. Wang, W. Zhou, W. Chen, R. G. Wu, L. Liu, D. Nath, and M. Y.-T. Leung, 2018: Revisiting the northern mode of East Asian winter monsoon variation and its response to global warming. *J. Climate*, **31**(21), 9001–9014, https://doi.org/10.1175/JCLI-D-18-0136.1.

Ham, S., and Y. Jeong, 2021: Characteristics of subseasonal winter prediction skill assessment of GloSea5 for East Asia. *Atmosphere*, **12**(10), 1311, https://doi.org/10.3390/atmos12101311.

He, S. P., and H. J. Wang, 2013a: Impact of the November/December Arctic Oscillation on the following January temperature in East Asia. *J. Geophys. Res.: Atmos.*, **118**(23), 12 981–12 998, https://doi.org/10.1002/2013JD020525.

He, S. P., and H. J. Wang, 2013b: Oscillating relationship between the East Asian winter monsoon and ENSO. *J. Climate*, **26**(24), 9819–9838, https://doi.org/10.1175/JCLI-D-13-00174.1.

Hersbach, H., and Coauthors, 2020: The ERA5 global reanalysis. *Quart. J. Roy. Meteor. Soc.*, **146**(730), 1999–2049, https://doi.org/10.1002/qj.3803.

Honda, M., J. Inoue, and S. Yamane, 2009: Influence of low Arctic sea-ice minima on anomalously cold Eurasian winters. *Geophys. Res. Lett.*, **36**(8), L08707, https://doi.org/10.1029/2008GL037079.

Huang, B. H., Z.-Z. Hu, and B. Jha, 2007: Evolution of model systematic errors in the Tropical Atlantic Basin from coupled climate hindcasts. *Climate Dyn.*, **28**(7–8), 661–682, https://doi.org/10.1007/s00382-006-0223-8.

Jhun, J.-G., and E.-J. Lee, 2004: A new East Asian winter monsoon index and associated characteristics of the winter monsoon. *J. Climate*, **17**(4), 711–726, https://doi.org/10.1175/1520-0442(2004)017<0711:ANEAWM>2.0.CO;2.

Jiang, D. B., D. Hu, Z. P. Tian, and X. M. Lang, 2020: Differences between CMIP6 and CMIP5 models in simulating climate over China and the East Asian monsoon. *Adv. Atmos. Sci.*, **37**(10), 1102–1118, https://doi.org/10.1007/s00376-020-2034-y.

Jiang, W. P., H. N. Gong, P. Huang, L. Wang, G. Huang, and L. S. Hu, 2022: Biases and improvements of the ENSO-East Asian winter monsoon teleconnection in CMIP5 and CMIP6 models. *Climate Dyn.*, **59**, 2467–2480, https://doi.org/10.1007/s00382-022-06220-5.

Jiang, X. W., S. Yang, Y. Q. Li, A. Kumar, W. Q. Wang, and Z. T. Gao, 2013: Dynamical prediction of the East Asian winter monsoon by the NCEP Climate Forecast System. *J. Geophys. Res.: Atmos.*, **118**(3), 1312–1328, https://doi.org/10.1002/jgrd.50193.

Kang, D., and M.-I. Lee, 2019: ENSO influence on the dynamical seasonal prediction of the East Asian winter monsoon. *Climate Dyn.*, **53**(12), 7479–7495, https://doi.org/10.1007/s00382-017-3574-4.

Kang, L. H., W. Chen, and K. Wei, 2006: The interdecadal variation of winter temperature in China and its relation to the anomalies in atmospheric general circulation. *Climatic and Environmental Research*, **11**(3), 330–339, https://doi.org/10.3969/j.issn.1006-9585.2006.03.009. (in Chinese with English abstract)

Kang, L. H., W. Chen, L. Wang, and L. J. Chen, 2009: Interannual variations of winter temperature in China and their relationship with the atmospheric circulation and sea surface temperature. *Climatic and Environmental Research*, **14**(1), 45–53, https://doi.org/10.3878/j.issn.1006-9585.2009.01.05. (in Chinese with English abstract)

Kerr, R. A., 2000: A North Atlantic climate pacemaker for the centuries. *Science*, **288**(5473), 1984–1985, https://doi.org/10.1126/science.288.5473.1984.

Kim, H.-M., P. J. Webster, and J. A. Curry, 2012: Seasonal prediction skill of ECMWF System 4 and NCEP CFSv2 retrospective forecast for the Northern Hemisphere Winter. *Climate Dyn.*, **39**(12), 2957–2973, https://doi.org/10.1007/S00382-012-1364-6.

Kim, J.-W., S.-I. An, S.-Y. Jun, H.-J. Park, and S.-W. Yeh, 2017: ENSO and East Asian winter monsoon relationship modulation associated with the anomalous northwest Pacific anticyclone. *Climate Dyn.*, **49**(4), 1157–1179, https://doi.org/10.1007/s00382-016-3371-5.

Li, C. Y., 1990: Interaction between anomalous winter monsoon in East Asia and El Niño events. *Adv. Atmos. Sci.*, **7**(1), 36–46, https://doi.org/10.1007/BF02919166.

Li, F., and H. J. Wang, 2012: Predictability of the East Asian winter monsoon interannual variability as indicated by the DEMETER CGCMS. *Adv. Atmos. Sci.*, **29**(3), 441–454, https://doi.org/10.1007/s00376-011-1115-3.

Li, J., B. Wang, and Y.-M. Yang, 2020: Diagnostic metrics for evaluating model simulations of the East Asian monsoon. *J. Climate*, **33**(5), 1777–1801, https://doi.org/10.1175/JCLI-D-18-0808.1.

Li, Y. Q., and S. Yang, 2010: A dynamical index for the East Asian winter monsoon. *J. Climate*, **23**(15), 4255–4262, https://doi.org/10.1175/2010JCLI3375.1.

Ma, T. J., and W. Chen, 2021: Climate variability of the East Asian winter monsoon and associated extratropical-tropical interaction: A review. *Annals of the New York Academy of Sciences*, **1504**(1), 44–62, https://doi.org/10.1111/nyas.14620.

MacLachlan, C., and Coauthors, 2015: Global Seasonal forecast system version 5 (GloSea5): A high-resolution seasonal forecast system. *Quart. J. Roy. Meteor. Soc.*, **141**(689), 1072–1084, https://doi.org/10.1002/qj.2396.

Mantua, N. J., S. R. Hare, Y. Zhang, J. M. Wallace, and R. C. Francis, 1997: A Pacific interdecadal climate oscillation with impacts on salmon production. *Bull. Amer. Meteor. Soc.*, **78**(6), 1069–1079, https://doi.org/10.1175/1520-0477(1997)078<1069:APICOW>2.0.CO;2.

Martin, G. M., R. C. Levine, J. M. Rodriguez, and M. Vellinga, 2021: Understanding the development of systematic errors in the Asian summer monsoon. *Geoscientific Model Development*, **14**(2), 1007–1035, https://doi.org/10.5194/gmd-14-1007-2021.

Megann, A., and Coauthors, 2014: GO5.0: The joint NERC-Met Office NEMO global ocean model for use in coupled and forced applications. *Geoscientific Model Development*, **7**(3), 1069–1092, https://doi.org/10.5194/gmd-7-1069-2014.

Mori, M., M. Watanabe, H. Shiogama, J. Inoue, and M. Kimoto, 2014: Robust Arctic sea-ice influence on the frequent

Eurasian cold winters in past decades. *Nature Geoscience*, **7**(12), 869–873, https://doi.org/10.1038/ngeo2277.

Park, T.-W., C.-H. Ho, and S. Yang, 2011: Relationship between the Arctic Oscillation and cold surges over East Asia. *J. Climate*, **24**(1), 68–83, https://doi.org/10.1175/2010JCLI3529.1.

Qiao, S. B., M. Zou, H. N. Cheung, W. Zhou, Q. X. Li, G. L. Feng, and W. J. Dong, 2020: Predictability of the wintertime 500 hPa geopotential height over Ural-Siberia in the NCEP climate forecast system. *Climate Dyn.*, **54**(3–4), 1591–1606, https://doi.org/10.1007/s00382-019-05074-8.

Qiao, S. B., M. Zou, H. N. Cheung, J. Y. Liu, J. Q. Zuo, Q. X. Li, G. L. Feng, and W. J. Dong, 2021: Contrasting interannual prediction between January and February temperature in southern China in the NCEP Climate Forecast System. *J. Climate*, **34**(7), 2791–2812, https://doi.org/10.1175/JCLI-D-20-0568.1.

Rae, J. G. L., H. T. Hewitt, A. B. Keen, J. K. Ridley, A. E. West, C. M. Harris, E. C. Hunke, and D. N. Walters, 2015: Development of Global Sea Ice 6.0 CICE configuration for the Met Office global coupled model. *Geoscientific Model Development*, **8**(7), 2529–2554, https://doi.org/10.5194/gmdd-8-2529-2015.

Reynolds, R. W., T. M. Smith, C. Y. Liu, D. B. Chelton, K. S. Casey, and M. G. Schlax, 2007: Daily high-resolution-blended analyses for sea surface temperature. *J. Climate*, **20**(22), 5473–5496, https://doi.org/10.1175/2007JCLI1824.1.

Scaife, A. A., and Coauthors, 2014: Skillful long-range prediction of European and North American winters. *Geophys. Res. Lett.*, **41**(7), 2514–2519, https://doi.org/10.1002/2014GL059637.

Sohn, S.-J., C.-Y. Tam, and C.-K. Park, 2011: Leading modes of East Asian winter climate variability and their predictability: An assessment of the APCC multi-model ensemble. *J. Meteor. Soc. Japan*, **89**(5), 455–474, https://doi.org/10.2151/jmsj.2011-504.

Sun, C. H., S. Yang, W. J. Li, R. N. Zhang, and R. G. Wu, 2016: Interannual variations of the dominant modes of East Asian winter monsoon and possible links to Arctic sea ice. *Climate Dyn.*, **47**(1), 481–496, https://doi.org/10.1007/s00382-015-2851-3.

Thompson, D. W. J., and J. M. Wallace, 1998: The Arctic Oscillation signature in the wintertime geopotential height and temperature fields. *Geophys. Res. Lett.*, **25**(9), 1297–1300, https://doi.org/10.1029/98GL00950.

Trenberth, K. E., 1997: The definition of El Niño. *Bull. Amer. Meteor. Soc.*, **78**(12), 2771–2778, https://doi.org/10.1175/1520-0477(1997)078<2771:TDOENO>2.0.CO;2.

Valcke, S., 2013: The OASIS3 coupler: A European climate modelling community software. *Geoscientific Model Development*, **6**(2), 373–388, https://doi.org/10.5194/gmd-6-373-2013.

Wallace, J. M., and D. S. Gutzler, 1981: Teleconnections in the geopotential height field during the northern hemisphere winter. *Mon. Wea. Rev.*, **109**(4), 784–812, https://doi.org/10.1175/1520-0493(1981)109<0784:TITGHF>2.0.CO;2.

Walters, D., and Coauthors, 2017: The Met Office unified model global atmosphere 6.0/6.1 and JULES global land 6.0/6.1 configurations. *Geoscientific Model Development*, **10**(4), 1487–1520, https://doi.org/10.5194/gmd-10-1487-2017.

Wang, B., R. G. Wu, and X. Fu, 2000: Pacific-East Asia teleconnection: How does ENSO affect East Asian climate? *J. Climate*, **13**(9), 1517–1536, https://doi.org/10.1175/1520-0442(2000)013<1517:PEATHD>2.0.CO;2.

Wang, B., Z. W. Zhu, C.-P. Chang, J. Liu, J. P. Li, and T. J. Zhou, 2010: Another look at interannual-to-interdecadal variations of the East Asian winter monsoon: The northern and southern temperature modes. *J. Climate*, **23**(6), 1495–1512, https://doi.org/10.1175/2009JCLI3243.1.

Wang, L., and W. Chen, 2010: How well do existing indices measure the strength of the East Asian winter monsoon? *Adv. Atmos. Sci.*, **27**(4), 855–870, https://doi.org/10.1007/s00376-009-9094-3.

Wang, L., and W. Chen, 2014: An intensity index for the East Asian winter monsoon. *J. Climate*, **27**(6), 2361–2374, https://doi.org/10.1175/JCLI-D-13-00086.1.

Wang, L., and M.-M., Lu, 2017: The East Asian winter monsoon. *The Global Monsoon System: Research and Forecast. 3rd ed.*, C.-P. Chang et al., Eds., World Scientific, 51–61.

Wang, L., W. Chen, and R. H. Huang, 2008: Interdecadal modulation of PDO on the impact of ENSO on the East Asian winter monsoon. *Geophys. Res. Lett.*, **35**(20), L20702, https://doi.org/10.1029/2008GL035287.

Watanabe, M., and T. Nitta, 1999: Decadal changes in the atmospheric circulation and associated surface climate variations in the northern hemisphere winter. *J. Climate*, **12**(2), 494–510, https://doi.org/10.1175/1520-0442(1999)012<0494:DCITAC>2.0.CO;2.

Wei, K., T. Xu, Z. C. Du, H. N. Gong, and B. H. Xie, 2014: How well do the current state-of-the-art CMIP5 models characterise the climatology of the East Asian winter monsoon? *Climate Dyn.*, **43**(5–6), 1241–1255, https://doi.org/10.1007/s00382-013-1929-z.

Wu, B. Y., and J. Wang, 2002: Winter Arctic Oscillation, Siberian High and East Asian winter monsoon. *Geophys. Res. Lett.*, **29**(19), 1897, https://doi.org/10.1029/2002GL015373.

Wu, B. Y., J. Z. Su, and R. H. Zhang, 2011: Effects of autumn-winter Arctic sea ice on winter Siberian High. *Chinese Science Bulletin*, **56**(30), 3220–3228, https://doi.org/10.1007/s11434-011-4696-4.

Zhang, D. Q., G. M. Martin, J. M. Rodríguez, Z. J. Ke, and L. J. Chen, 2020a: Predictability of the western North Pacific subtropical high associated with different ENSO phases in GloSea5. *J. Meteorol. Res.*, **34**(5), 926–940, https://doi.org/10.1007/s13351-020-0055-1.

Zhang, P., Z. W. Wu, and J. P. Li, 2019: Reexamining the relationship of La Niña and the East Asian Winter Monsoon. *Climate Dyn.*, **53**(1), 779–791, https://doi.org/10.1007/s00382-019-04613-7.

Zhang, P., Z. W. Wu, J. P. Li, and Z. N. Xiao, 2020b: Seasonal prediction of the northern and southern temperature modes of the East Asian winter monsoon: tThe importance of the Arctic sea ice. *Clim.ate Dyn.*, **54**(D147), 3583–3597, https://doi.org/10.1007/s00382-020-05182-w.

Zhang, R. H., A. Sumi, and M. Kimoto, 1996: Impact of El Niño on the East Asian Monsoon: A diagnostic study of the '86/87 and '91/92 events. *J. Meteor. Soc. Japan*, **74**(1), 49–62, https://doi.org/10.2151/jmsj1965.74.1_49.

Zhou, W., X. Wang, T. J. Zhou, C. Li, and J. C. L. Chan, 2007: Interdecadal variability of the relationship between the East Asian winter monsoon and ENSO. *Meteorol. Atmos. Phys.*, **98**(3–4), 283–293, https://doi.org/10.1007/s00703-007-02

63-6.

Zhu, Y. F., 2008: An index of East Asian winter monsoon applied to description the Chinese mainland winter temperature changes. *Acta Meteorologica Sinica*, **66**(5), 781−788, https://doi.org/10.11676/qxxb2008.071. (in Chinese with English abstract)

Zou, M., and Coauthors, 2022: Predictability of the two temperature modes of the East Asian winter monsoon in the NCEP-CFSv2 and MRI-CPSv2 models. *Climate Dyn.*, **59**(11−12), 3211−3225, https://doi.org/10.1007/s00382-022-06254-9.